Lab on a Chip

PAPER

View Article Online
View Journal | View Issue

Cite this: *Lab Chip*, 2022, **22**, 2352

Quantitative isothermal amplification on paper membranes using amplification nucleation site analysis†

Benjamin P. Sullivan, [a] Yu-Shan Chou,[b] Andrew T. Bender, [a] Coleman D. Martin, [b] Zoe G. Kaputa,[c] Hugh March,[c] Minyung Song[a] and Jonathan D. Posner *[abd]

Received 4th January 2022,
Accepted 26th April 2022

DOI: 10.1039/d2lc00007e

rsc.li/loc

Quantitative nucleic acid amplification tests (qNAATs) are critical in treating infectious diseases, such as in HIV viral load monitoring or SARS-CoV-2 testing, in which viral load indicates viral suppression or infectivity. Quantitative PCR is the gold standard tool for qNAATs; however, there is a need to develop point-of-care (POC) qNAATs to manage infectious diseases in outpatient clinics, low- and middle-income countries, and the home. Isothermal amplification methods are an emerging tool for POC NAATs as an alternative to traditional PCR-based workflows. Previous works have focused on relating isothermal amplification bulk fluorescence signals to input copies of target nucleic acids for sample quantification with limited success. In this work, we show that recombinase polymerase amplification (RPA) reactions on paper membranes exhibit discrete fluorescent amplification nucleation sites. We demonstrate that the number of nucleation sites can be used to quantify HIV-1 DNA and viral RNA in less than 20 minutes. An image-analysis algorithm quantifies nucleation sites and determines the input nucleic acid copies in the range of 67–3000 copies per reaction. We demonstrate a mobile phone-based system for image capture and onboard processing, illustrating that this method may be used at the point-of-care for qNAATs with minimal instrumentation.

1. Introduction

Nucleic acid amplification tests (NAATs) are critical tools in diagnosing infectious diseases due to their unparalleled specificity and sensitivity. Quantitative nucleic acid amplification tests (qNAATs) quantify target nucleic acids (NA) concentrations in biological samples. This is crucial in many applications, including HIV viral load testing where NA concentrations (*i.e.* viral load) are related to viral suppression and transmission risk. HIV-positive individuals with viral loads of less than 1000 copies of viral RNA per mL of plasma have significantly better health outcomes and reduced risk of transmitting HIV to partners.[1–3] Recently, SARS-CoV-2 viral load measurements have been related to infectivity, with higher viral loads being strongly correlated to cultivable virus.[4,5] Quantification of pathogen load can be crucially important in triaging and determining appropriate clinical care.

Quantitative PCR (qPCR) is the gold standard for quantifying NAs and amplifies pathogenic nucleic acids using precise thermocycling for denaturation, annealing, and extension of duplicated DNA. qPCR provides quantification over 9 orders of magnitude relative to known quantities of DNA. Digital droplet PCR (ddPCR) has emerged as the most precise method for absolute NA quantification. It leverages Poisson statistics with thousands of discrete PCR amplification reactions to provide absolute sample quantification.[6,7] ddPCR typically has lower dynamic range than qPCR (5+ orders of magnitude for commercial systems such as the BioRad QX200 (ref. 8)) due to signal saturation and requires separate droplet generation prior to amplification cycling. Both qPCR and ddPCR are traditionally restricted to well-instrumented laboratories or hospitals due to cold chain dependent reagents, delicate instrumentation, reliable electrical power, proficient laboratory staff, and appropriate infrastructure to host required equipment.[9]

Pathogen quantification using qPCR or ddPCR in outpatient or low- and middle-income country clinics is

[a] *Department of Mechanical Engineering, University of Washington, Stevens Way, Box 352600, Seattle, WA 98195, Washington, USA. E-mail: jposner@uw.edu*
[b] *Department of Chemical Engineering, University of Washington, Seattle, Washington, USA*
[c] *Paul G. Allen School of Computer Science & Engineering, University of Washington, Seattle, Washington, USA*
[d] *Department of Family Medicine, University of Washington, Seattle, Washington, USA*

† Electronic supplementary information (ESI) available. See DOI: https://doi.org/10.1039/d2lc00007e

challenging due to the logistics around specimen collection, transport, batched testing, and the return of results to clinicians and patients (in addition to the aforementioned restriction to centralized laboratories).[10] In outpatient clinics, this can result in delayed diagnoses that prevent immediate linkage to appropriate treatment or lead to loss-to-follow-up.[11,12] Consequently, there is an unmet need to develop inexpensive point-of-care (POC) qNAATs, particularly in low- and middle-income countries (LMIC).[9,10] Isothermal amplification methods are emerging as an alternative to PCR, as they require significantly less instrumentation and produce results much more quickly than PCR. Instead of relying on thermocycling up to 95 °C, isothermal amplification techniques leverage unique enzymes and/or primer design for nucleic acid replication at a single temperature of 60 °C or below. The elimination of thermocycling requirements also removes the inherent annealing/extension synchronization that gives qPCR its precise quantification capability, making sample quantification *via* isothermal amplification challenging.[13] Loop-mediated isothermal amplification (LAMP) is a popular amplification method that is performed at 60–65 °C for 30–60 minutes. Several groups have related various metrics, such as real-time reaction turbidity or end-point colorimetric indicator dyes to input nucleic acid copy numbers.[14,15] Recombinase polymerase amplification (RPA) is a particularly attractive amplification method at the point-of-care because it is performed at a single low temperature (39 °C) and produces results in less than 20 minutes. Most RPA assays use bulk fluorescence measurement (*e.g.* time-to-threshold) for nucleic acid quantification, though this approach lacks precision and calibrations can vary across target genotype/subtype.[16–19] Challenges in quantification by RPA have been attributed to desynchronized amplification, chemical initiation of the reaction, and high viscosity reaction chemistry.[13] Some efforts to use RPA for quantification, such as those shown by Crannell *et al.* and Bender *et al.*, have had some success, though there are no careful studies showing that RPA has sufficient quantitative precision for clinical applications.[20,21]

Isothermal amplification has also been used in digital amplification schemes using individual droplets or wells in microfluidic devices for absolute quantification of nucleic acids.[22–24] Similar to ddPCR, these digital methods use binary determination of amplification in each individual well or droplet combined with Poisson distribution statistics. This approach requires that individual small aqueous reaction volumes be generated, for example, using a microfluidic device for droplet generation in a immiscible oil carrier phase,[25] or sliding chip that compartmentalizes small volumes in wells, such as the SlipChip.[22,26] These digital isothermal amplification methods demonstrate repeatable outputs with precise and accurate quantification, though they all require specialized chips, emulsion generators, and/or complex loading procedures that potentially increase costs and complicate POC applications.

Paper-based POC NAATs devices have leveraged isothermal amplification within commercially available porous substrates.[21,27–30] This approach has been developed with the goal of reducing test cost and complexity as well as increasing their robustness. Much of this paper-based work has focused on qualitative tests; however some effort has been made to extract quantitative or semi-quantitative information about input nucleic acid concentration.[21,30–32] Lateral-flow readout has been used with some success for order-of-magnitude semi-quantitative isothermal nucleic acid amplification. A range of isothermal chemistries (RPA,[33–35] LAMP,[36,37] and HDA[38]) have been amplified in tubes[33,34,36] or in membranes[37,39] and then read out using lateral flow strips, with line intensity (or some ratio of line intensities) being used to provide quantification. Very recently, tunable competitive internal controls have been added into amplification reactions to further improve quantification, such as those shown by Hull *et al.* and Rosenbohm *et al.*[33,34,38] These methods demonstrate quantification across several orders of magnitude (the competitive internal control can be tuned to extend this range if multiple parallel reactions are used), though at the cost of increased assay complexity and user steps.

Fluorescence-based assays with various isothermal amplification chemistries have also been used in paper-based NAATs, with bulk fluorescent signals related to sample concentration, similar to traditional tube-based assays.[21,27,29,40–42] These previous works have used both liquid and lyophilized isothermal amplification chemistries, and show correlations between bulk endpoint fluorescence and input copy number across 4–6 orders of magnitude; however there is typically significant variation in output signal that makes precise quantification challenging, even across orders of magnitude. As others have pointed out, this is likely due to the sensitivity of isothermal amplification to various random perturbations and effects of non-specific amplification products.[34] Collectively, these previous strategies fail to show adequately precise quantification of isothermal amplification methods in low-cost paper-based devices that can be used at the point-of-care, and warrant investigation into other, novel strategies for quantification.

In this work, we report a paper-based, isothermal nucleic acid amplification test that quantifies input HIV-1 RNA and DNA by leveraging distinct regions of fluorescent amplification products. We show that RPA reactions in paper membranes produce discrete amplification nucleation sites and that the number of amplification sites correlates to input NA concentrations. We develop and use image analysis algorithms to quantify RNA and DNA in the range of 67–3000 copies per reaction in less than 20 minutes at a constant 39 °C. We demonstrate a mobile phone-based image capture system with onboard image processing using a custom Android app, showing that this method may be well suited for point-of-care applications.

2. Methods

2.1 Amplification on membranes

RPA and RT-RPA reactions are performed on a variety of commercially available porous membranes (Millipore GF041, Whatman GF/DVA, Whatman Fusion 5, and Millipore PES GPWP04700). We first cut the membranes with a flatbed cutter (FCX4000-50ES, Graphtec America, Inc., USA) into squares to accommodate a 50 μL RPA reaction volume. Dimensions of the squares differed with respect to each membrane's respective water absorbency, with side lengths of 11.2 mm, 7.2 mm, 12.7 mm, and 13.4 mm, for the GF041, GF/DVA, Fusion 5, and PES membranes, respectively.

The Millipore PES GPWP04700 membrane tears when cut by the flatbed cutter, so these membranes are cut with a CO_2 laser (PLS6.150D, Universal Laser Systems, USA). The low water absorbency of the PES membrane necessitates a square pad with a 25 μL capacity to prevent an excessively large imaging area.

Amplification pads are placed into a 60 × 15 mm polystyrene Petri dish (25384-092, VWR, USA), and a 50 μL RPA reaction (mastermix and target) is pipetted evenly onto the pad (25 μL in the case of PES). The amplification pad is then covered with PCR tape (TempPlate RT Select Optical Film, USA Scientific, USA), ensuring good sealing adhesion between the PCR tape and the Petri dish. We lid the Petri dish and seal along its edges with Parafilm M (Millipore Sigma, USA) to prevent contamination *via* aerosolized amplification products. The Petri dish is placed on a resistive heater (Mr. Coffee, USA) that is set to 39 °C using an external PID temperature controller with a Type-K thermocouple attached to the heating surface. The reaction is imaged for 20 minutes and then the Petri dish is sealed in a plastic bag and disposed of. The experimental process is shown in Fig. 1.

2.2 RPA and RT-RPA conditions

In RPA experiments, we targeted synthetic DNA (gBlocks Gene Fragments, Integrated DNA Technologies, USA) that contains 1000 base pairs of the HIV-1 genome (group M, subtype A). For RT-RPA experiments, we targeted purified HIV RNA from HIV-1 supernatant, prepared as described in Lillis *et al.*[19] Briefly, HIV-1 supernatant (group M, subtype A, NCBI accession number: JX140650) was received from the External Quality Assurance Program Oversight Laboratory at Duke University,[43] and extracted using QIAamp Viral RNA Mini Kits (Qiagen, DEU). The resulting viral RNA was quantified *via* quantitative real-time PCR. Both target types were diluted with DEPC-treated water to create dilution series used in establishing quantifiable ranges for amplification nucleation site analysis.

In both RPA and RT-RPA, we use primers and probe developed by Lillis *et al.* for cross-subtype HIV-1 detection.[19] The amplification mastermix consists of a TwistAmp exo kit lyophilized pellet (TwistDx, GBR), 29.5 μL rehydration buffer, 14 mM magnesium acetate, 540 nM forward and reverse primer (Integrated DNA Technologies, USA), and 120 nM exo-probe (LGC Biosearch Technologies, GBR). In the case of RT-RPA experiments, 0.08 U μL^{-1} reverse transcriptase is added (OmniScript, Qiagen, DEU). The TwistAmp exo kit instructions are otherwise followed up until incubation. Briefly, the mastermix of rehydration buffer, primers, probe, and RT (in the case of RT-RPA) is added to a lyophilized exo-kit RPA pellet, rehydrating it. We then add the target (DNA or RNA) to the mastermix and add 2.5 μL MgOAc (280 mM) to the cap lid of the tube. The tube is then closed and shaken manually for ~30 seconds to start the reaction and ensure homogenous distribution of reactants. We then immediately open the tube and pipette the 50 μL reaction volume evenly onto an amplification pad. In the case of tube-based experiments, the tubes are placed into a T16-ISO instrument (Axxin, USA), which incubates the tubes at 39 °C and records fluorescence for 20 minutes, with a manual mixing step at 4 minutes. To test for the presence of proviral DNA in the extracted viral RNA, we performed tube-based RPA experiments using the viral RNA in which reverse transcriptase was purposefully left out; these experiments did not amplify.

2.3 Imaging and data analysis

An epifluorescence fluorescence microscope (AZ100, Nikon, JPN) with 0.5× objective and illumination system (X-Cite exacte, Excelitas Technologies, USA) images the RPA nucleation site evolution in the pad. The 0.5× objective used

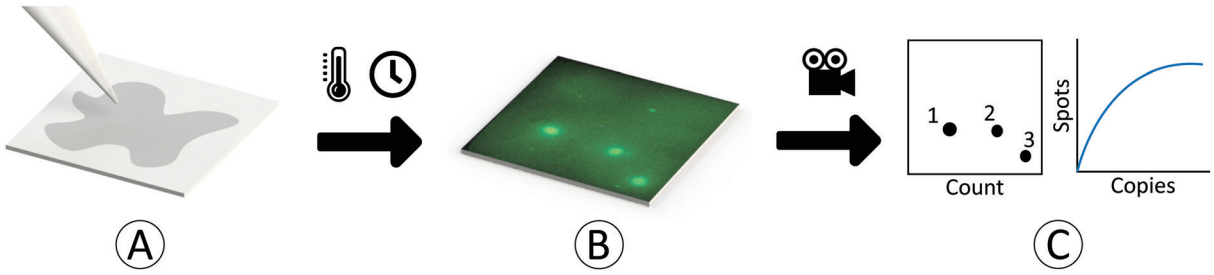

Fig. 1 Process flow for amplification nucleation site quantification and analysis. (A) Recombinase polymerase amplification mastermix and target are dispensed onto paper membrane. The membrane is covered with PCR tape and heated to 39 °C for 20 minutes. (B) Discrete amplification nucleation sites begin to form and are recorded *via* fluorescent microscopy. (C) The images are analyzed by an image analysis algorithm which quantifies the number of amplification nucleation sites. This value is related to the original sample target concentration.

has a field of view diameter of 43 mm. We use an epifluorescence filter cube set (XF100-2, Omega Optical, LLC., USA) and capture grayscale images every second for 20 minutes using a CMOS camera (Prime BSI Express, Teledyne Photometrics, USA).

A custom image analysis algorithm (MATLAB, MathWorks, USA) counts the number of amplification nucleation sites over the full 1200 frame image-stack. The algorithm first resamples the image-stack, effectively doubling the pixel density, then averages the pixel intensity over every 10 frames to reduce image noise. It applies background subtraction to the entire image-stack by averaging the frames in the first 2 minutes and subtracting this resulting average frame from all subsequent frames on a pixel-by-pixel basis to eliminate any artifacts caused by auto-fluorescence of the amplification membranes, PCR tape, or Petri dish. A circle-finding function (based on a Circular Hough Transform algorithm) identifies discrete amplification nucleation sites for each frame. A moving-mean smoothing function averages the number of amplification nucleation sites over time using a 5-frame window, as inherent pixel noise can result in deviations in number of identified sites from frame to frame. The maximum smoothed number of sites identified over the 20 minutes is used as the number of amplification nucleation sites for that experiment. We refer to this method as the CHT (Circular Hough Transform) method. An alternative algorithm that relies on thresholding to identify the nucleation sites is also used. This algorithm (coded *via* ImageJ[44]) averages the pixel intensity over every 10 frames, and then performs a rolling-ball background subtraction. Thresholding of the resulting image-stack is performed using Otsu's method, followed by a watershed transformation to separate merged nucleation sites, and then analysis *via* an edge-finding algorithm to identify distinct nucleation sites. We refer to this method as the TAP (Threshold Analyze Particles) method. Both codes are available in the ESI.†

We also use a mobile phone to image RPA nucleation sites to demonstrate the potential use of this method in point-of-care environments. We use a Pixel 4A mobile phone (Google, USA), bandpass excitation filter (FF01-466/40-25, Semrock, USA), bandpass emission filter (FF01-550/49-25, Semrock, USA), and plano-convex macro lens (37-784, Edmund Optics, USA). The excitation and emissions bandpass filters are centered at 466 nm and 550 nm, respectively, for use with the FAM fluorophore family. The plano-convex lens is positioned such that it is directly adjacent to the mobile phone's camera, while the excitation and emission filters are positioned underneath the mobile phone flash and camera, respectively. These are held in position by a 3D-printed fixture (S3, Ultimaker, NLD), as shown in Fig. 2. The experiments were conducted in a darkroom to avoid any ambient light. Images were acquired with a fixed setting of ISO 55 and an exposure of 4 seconds.

We analyze a single frame recorded at 750 seconds into an experiment with a custom Android app written in Python 3.8.10 using the OpenCV library and run *via* Python for Android.[45] The algorithm first employs an auto-cropping function to define the square region of interest containing the amplification pad. A contrast limited adaptive histogram equalization adjusts the contrast of the image, and a bilateral filter smooths the image while also removing pixel noise. The image is binarized *via* an adaptive Gaussian binary threshold, and a Hough circle transform then identifies and quantifies the discrete nucleation sites. The user interface displays a results screen featuring the experimental image with nucleation sites highlighted, determination of HIV status, number nucleation sites identified, and corresponding nucleic acid copies (Fig. 2C).

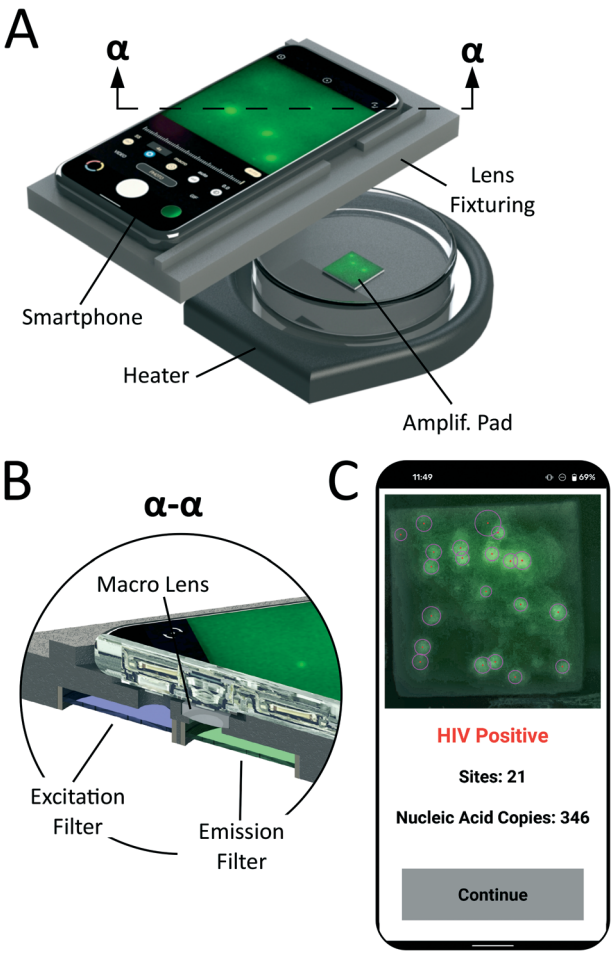

Fig. 2 Mobile phone experimental setup for nucleation site analysis, showing (A) mobile phone, Petri dish containing the amplification membrane, heater, and 3D-printed fixturing, which holds the (B) excitation and emission filters, as well as the plano-convex macro lens. (C) Onboard processing of the images is performed using a custom app which displays the number of sites counted and calculates the estimated nucleic acid copies present.

3. Results and discussion

We perform RPA and RT-RPA on GF/DVA membranes for a range of target concentrations (30–100 000 cps rxn^{-1} and 50–3000 cps rxn^{-1} for DNA and RNA, respectively). At target

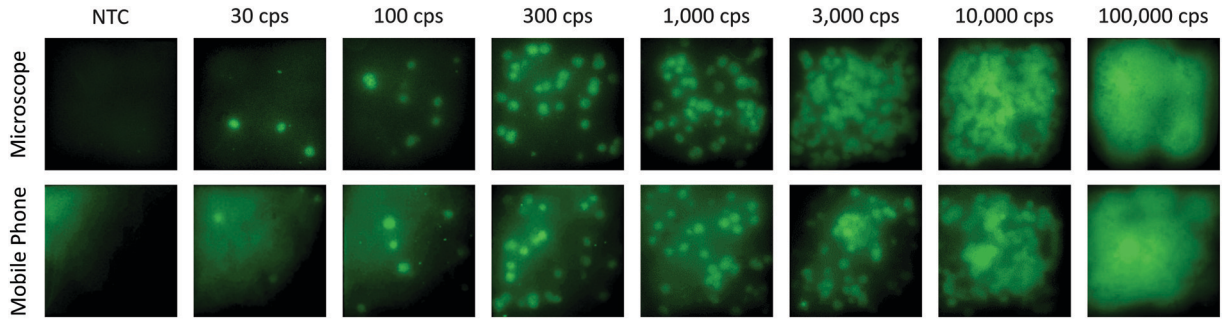

Fig. 3 Representative fluorescence images of RPA amplification of HIV-1 DNA on GF/DVA membrane captured using a microscope and mobile phone with copy number ranging from 30 to 100 000 cps rxn^{-1}. Images were recorded at t = 750 s. at lower copy numbers (30–3000 cps rxn^{-1}), we observe discrete amplification nucleation sites, with a positive relationship between number of nucleation sites and input copy number. At high copy numbers (10 000 and 100 000 cps rxn^{-1}), the nucleation sites are numerous and they merge into a splotchy heterogenous fluorescence image, making quantification difficult.

concentrations of 30–3000 cps rxn^{-1} of DNA and RNA, we observe spatially separated and distinct fluorescent amplification nucleation sites dispersed on the amplification pad that grow in diameter over the course of the experiment, as shown in Fig. 3. At higher concentrations (>10 000+ cps rxn^{-1}), there are many closely packed nucleation sites that merge, resulting in splotchy heterogenous fluorescence over the amplification pad and making individual site identification more challenging.

To our knowledge, this is the first instance that individual amplification nucleation sites in paper membranes have been described in the literature. We did not evaluate other amplification chemistries, though other publications that use these methods (*e.g.* LAMP, iSDA, *etc.* on paper membranes) exhibit homogenous fluorescence increase and not discrete amplification nucleation sites.[29,41,46–48] We hypothesize that the nucleation sites are a result of amplification reactants (*e.g.* recombinase-primer filaments) or products (*i.e.* duplicated amplicons) diffusing slowly in and out of the amplification nucleation sites. RPA's high viscosity reaction buffer likely impedes diffusion of reactants and products, limiting the reaction to individual nucleation sites. RPA relies on viscous crowding agents such as polyethylene glycol to increase enzyme catalytic efficiency,[49] which traditionally necessitates a mixing step halfway through tube-based RPA assay protocols.[49,50] Previously, cast-gel amplification systems, including in-gel LAMP or in-gel PCR, have been leveraged in a similar application.[51,52] In these systems, native amplification chemistries are mixed with cross-linking polymers (*e.g.* polyacrylamide gels) resulting in discrete amplification zones. In the work presented here, the highly viscous RPA amplification chemistry in the porous membrane micron scale geometries dampen fluid flow[53,54] resulting in a diffusion-limited transport and formation of discrete amplification sites.

We find significant differences between the RPA reactions in the various membranes tested. For our initial comparison tests, we use 1000 cps HIV-1 DNA per reaction as the target. Both the GF041 and GF/DVA membranes show robust amplification, with 34–50 amplification nucleation sites visible. The Fusion 5 only results in 1–2 amplification nucleation sites and marginal increase in overall fluorescence. The PES GPWP04700 membrane supports successful amplification, in agreement with previous studies.[27,55] We find that both the GF041 and PES membranes exhibit lower contrast between the background and amplification fluorescence in comparison to the GF/DVA membrane. Due to the robust amplification and superior contrast, all subsequent experiments were carried out using the Whatman GF/DVA membrane. Representative images of comparison RPA reactions on the various membranes are shown in Fig. S1 in the ESI.†

Fig. 4A shows example images captured *via* fluorescent microscope and processed with the CHT method, including the raw image, resampled image, multi-frame averaged image, background subtraction, and identified sites. We plot the number of nucleation sites counted for the algorithms we tested compared to the number of sites counted manually. We find that CHT, TAP, and manual count methods agree well at low copy numbers (<300 cps rxn^{-1}), where there are relatively few (<50) amplification nucleation sites. At higher DNA copy numbers (1000–3000 cps rxn^{-1}), there are differences between the algorithmic counts and manual counts, though this disagreement is scattered. At higher copy number (10 000 cps rxn^{-1}), both algorithms significantly undercount the number of sites relative to the manual count. We believe this deviation is due to the algorithms being unable to robustly identify individual nucleation sites prior to the sites merging at higher input copy numbers. This is supported by plots of identified amplification nucleation sites over time of a single experiment, shown in Fig. 4C. Often, the number of nucleation sites will peak halfway through an experiment (we use the maximum as the recorded value for each respective experiment) and then begin to decrease as the sites merge, revealing this weakness in the algorithms (additional nucleation sites *vs.* time plots are shown in the ESI†). In all subsequent microscope-based experiments, we use the CHT algorithm for nucleation site quantification.

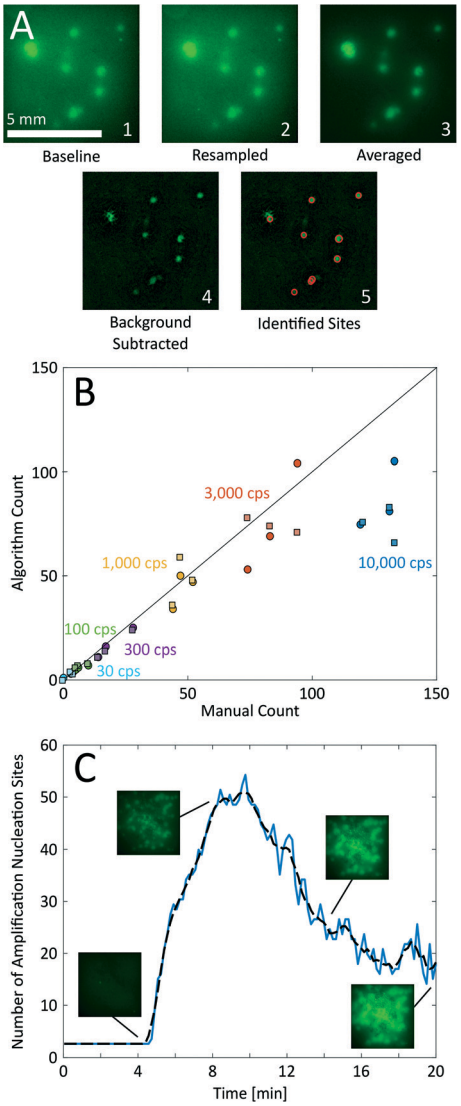

Fig. 4 Results of algorithmic nucleation site identification and counting. (A) Circular Hough Transform (CHT) algorithm process performed on microscope-acquired images. The raw data (1) is first resampled to increase pixel density (2) with the pixel intensity averaged over 10 frames (3). we perform background subtraction (4), subtracting the average of the first two minutes' frames on a pixel-by-pixel basis with the resulting amplification nucleation sites then identified and quantified *via* a circle counting algorithm (5). (B) Comparison of the CHT (○) and TAP (□) algorithms against a manual count of RPA amplification nucleation sites with DNA target copy numbers of 30–10 000 cps rxn^{-1}. At lower copy numbers (≤3000 cps rxn^{-1}), there is good agreement between the manual count and both algorithms. In this regime, the number of amplification nucleation sites is relatively low and there is sufficient separation between the sites for successful algorithmic quantification. At higher copy numbers (10 000 cps rxn^{-1}), the nucleation sites begin to merge, making algorithmic quantification more difficult and resulting in an undercount relative to the manual count. This undercount is observed for both algorithms, though it is more pronounced in the tap algorithm. (C) Representative experiment of 1000 cps rxn^{-1} DNA on Whatman GF/DVA membrane, showing the number of amplification nucleation sites as a function of experiment time, quantified *via* the CHT image analysis algorithm. A sharp increase in number of nucleation sites occurs near 4–10 minutes, followed by a decrease in number of identified sites as the sites begin to grow and merge. The dashed line represents the moving-mean smoothing function used.

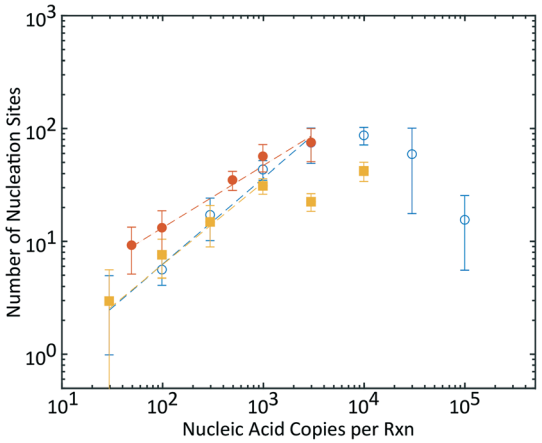

Fig. 5 Quantification of amplification nucleation sites for HIV DNA (blue open circles) and RNA (red filled circles) on GF/DVA membrane captured using a microscope compared to HIV DNA data captured and processed using a mobile phone (yellow filled squares). Data points represent the average and standard deviations (n = 3) for each target copy number tested and quantified using CHT algorithms. Dashed lines represent fitted models in all cases, we observe a strong relationship between nucleic acid input copy number and number of amplification nucleation sites. At high copy numbers (>10 000 cps rxn^{-1}), the number of measured nucleation sites decreases due to merging of amplification sites and inability of the experimental methodology to resolve and quantify the individual nucleation sites.

In Fig. 5 we plot the number of nucleation sites as a function of the number of nucleic acid copies per reaction for HIV-1 DNA and RNA using both the microscope and mobile phone imaging systems. The data shows that the number of amplification nucleation sites is proportional (log–log) to the number of input target copies. For RPA experiments with DNA target, input copy numbers of 30–100 000 cps rxn^{-1} were tested in triplicates and all experiments showed positive amplification except for one trial at 30 cps rxn^{-1}. No template controls (NTCs) did not show any amplification. We estimate the limit of detection (LoD) of this method *via* Probit analysis[56] as copies DNA per reaction. We find that the number of amplification nucleation sites as a function of copies of DNA per reaction follows power-law relationship in the form of $y = b \times x^m$, where b = 0.184 and m = 0.766. This relationship holds well up to 3000 cps rxn^{-1}, after which the number of measured amplification nucleation sites reaches a maximum and then decreases with increasing number of copies. The measured decrease in amplification sites is due to merging of sites at high copy numbers (10 000–100 000 cps rxn^{-1}) and the inability of the algorithms to capture and record all the nucleation sites. With our methodology, we report the dynamic range to be 67–3000 copies of HIV-1 DNA per reaction (equivalent to 1300–60 000 cps mL^{-1}). We show a comparison plot with a manual count in Fig. S6,† showing an extended dynamic range of up to 10 000 cps rxn^{-1}, suggesting that algorithm optimization can likely extend the reported dynamic range. Note that it is difficult to perform manual counts at copy numbers upwards of 10 000 cps rxn^{-1}, as the nucleation sites

have already merged once they become sufficiently bright to distinguish from the background. These results suggest that alternative algorithm methodologies, such as pattern recognition or machine learning, may be useful in extending the dynamic range. While this site merging behavior limits the current dynamic range, we are still able to determine successful amplification in high copy number experiments using bulk fluorescence values.

Similar discrete amplification nucleation sites are observed in the RT-RPA experiments with HIV-1 RNA target. The concentrations of viral RNA tested included 50–3000 cps rxn^{-1}. We fit a similar power law model to the data ($y = b \times x^m$), where $b = 1.047$ and $m = 0.551$.

The mobile phone-based imaging and processing method demonstrates similar performance to microscope-based image capture for 30–1000 cps rxn^{-1}; however, the performance of this system degrades at roughly 3000 cps rxn^{-1}, significantly lower than the microscope-based system. This reduction in the dynamic range is due to the reduced sharpness and signal-to-noise of the mobile phone-based images and the associated challenges in counting the sites. The power law model fit to the data, ranging from 30–1000 cps rxn^{-1}, is in the form $y = b \times x^m$, where $b = 0.215$ and $m = 0.731$. The fit parameters are remarkably close to the fit calculated for the microscope-acquired data. In this work, we use a designated dark room to exclude ambient light. In a point-of-care setting, a specially constructed enclosure or dark box would be required and interface directly with the smart phone while holding the necessary optics, similar to previously used dark boxes for epifluorescence imaging.[57]

We compare the LOD, dynamic range, time, cost, and complexity of amplification nucleation site analysis to ddPCR and various other isothermal amplification techniques in Table 1. ddPCR has the lowest limit-of-detection (1 copy per 20 μL reaction volume) and the largest dynamic range of the digital methods reviewed here (5 orders of magnitude), though requires multiple devices (droplet generator, thermocycler, and droplet reader) which cost upwards of $100 000. Other digital methods, such as the SlipChip[22] have marginally poorer performance than ddPCR, with LODs in the range of 1000 to 10 000 cps mL^{-1} and similar high end dynamic range. While some of these chip-based platforms may ultimately be less expensive than commercially available ddPCR systems, they are manufactured *via* photolithography, complicating widespread POC applications. Publications using bulk fluorescence magnitudes of isothermal amplification for quantification report dynamic ranges of 3 to 4 orders of magnitude and 20–30 minute test time. Here, we report a minimally instrumented isothermal amplification which can quantify input copies over a dynamic range of 1.5 orders of magnitude.

While this method in its current form has smaller dynamic range compared to other digital methods, bulk fluorescence measurements of the amplification pad can be used to determine positive amplification at input concentrations above the quantifiable levels. Serial dilution

Table 1 Comparison of amplification methods to quantify pathogen concentration

Publication	Description	Reported range	Manufacturing	Time to results	Quantification scheme	Notes
Bio-RAD QX200	ddPCR	5×10 to 6×10^6 cps mL^{-1}		120 minutes	Digital Poisson statistics	Requires separate droplet generator, thermocycler, and reader, $100 000 cost
Shen *et al.*[22]	Digital RPA performed on SlipChip microfluidic chip	1.4×10^3 to 1×10^6 cps mL^{-1}	Photolithography	60 minutes	Digital Poisson statistics	Used 1550 nanoliter-sized wells with automatic filling
Li *et al.*[23]	Digital RPA performed on microfluidic chip	1.3×10^4 to 2.9×10^6 cps mL^{-1}	Photolithography	20 minutes	Digital Poisson statistics	Used 27 000 picoliter-sized wells, rather complicated loading procedure
Lin *et al.*[24]	Digital LAMP on track-etched membrane	1.1×10^4 to 1.1×10^8 cps mL^{-1}	LAMP mastermix added directly to polycarbonate membrane	40 minutes	Digital Poisson statistics	Leveraged membrane pore structure to discretize amplification reactions
Liu *et al.*[41]	Paper-based LAMP	1×10^6 to 1×10^{10} cps mL^{-1}	Lyophilized reagents on glass fiber membrane	30 minutes	Time-to-threshold analysis	Developed separate reader to measure real-time fluorescence
Seok *et al.*[29]	Paper-based LAMP	5.9×10^3 to 5.9×10^6 cps mL^{-1}	Dried LAMP reagents on polyethersulfone membrane	60 minutes	Bulk fluorescence magnitude	Multiplexed detection *via* multiple amplification pads
Ahn *et al.*[27]	Paper-based RPA	1×10^2 to 1×10^5 cfu mL^{-1}	Dried RPA reagents on polyethersulfone membrane	20 minutes	Bulk fluorescence magnitude	Multiplexed detection *via* multiple amplification pads, able to distinguish orders of magnitude input CFU concentrations
This work	Paper-based RPA	1.3×10^3 to 6×10^4 cps mL^{-1}	RPA mastermix added directly to glass fiber membrane	20 minutes	Amplification nucleation site analysis	No alterations to the membrane required, mobile phone-compatible

of the target sample may be used with multiple concurrent amplification reactions (on separate amplification pads) to extend the dynamic range, with the only limitation being space and sample volume limits. This parallel processing of several target sample dilutions is routinely employed with ddPCR, which also suffers from signal saturation at the upper end of its dynamic range. Additional image processing methods, such as convolutional neural networks or similar image analysis machine learning algorithms might be employed to increase the dynamic range as well, potentially taking advantage of nucleation site cluster formation visible at higher input copy numbers, as opposed to individual nucleation site counting.[51]

Amplification nucleation site analysis may provide sufficient precision and accuracy for some point-of-care nucleic acid quantification applications. For example, in HIV-1 viral load monitoring the relevant quantification range of interest is 200–1 000 000 cps mL^{-1} (whereas the current dynamic range we show of 67–3000 cps rxn^{-1} equates to 1300–60 000 cps mL^{-1}).[10] We note that in this work, we tested highly purified and simple samples and a complete POC diagnostic test may require significant sample preparation steps that impact the concentration of target in the reaction volume. Nucleation site counting may also provide greater precision and accuracy than tube-based RPA. As an estimate, we use the calculated calibration curve and determine the average predicted concentrations and associated standard deviations ($n = 3$) for the collected data, similar to the process used by Crannell *et al.*[20] and shown in Table 2. Full calculations and tube-based RPA results are shown in the ESI.† Tube-based RPA is able to reasonably quantify both HIV-1 DNA and viral RNA within 0.33 and 0.25 $\log_{10}$ (copies per reaction) of the correct concentration on average for DNA and RNA respectively, within the dynamic range tested, in agreement with results shown in Crannell *et al.*[20] For the same concentrations, microscope-acquired amplification nucleation site analysis quantifies the samples within 0.14 and 0.16 $\log_{10}$ (copies per reaction) of the correct concentration on average for DNA and RNA targets, respectively. The RPA amplification nucleation site analysis exceeds the ideal product attributes for a HIV POC viral load test for quantification precision.[10]

Amplification nucleation site analysis might also aid in quantification of RPA reactions that are slowed relative to calibration curves created with pristine and controlled/contrived target sequences. While RPA is well-known for its ability to robustly amply across genotypes and subtypes by withstanding primer mismatches,[13,58] mismatches can have a significant effect on amplification rate and time-to-threshold.[19] This compounds challenges in tube-based quantification if exact target sequence is not known *a priori*, for example, when multiple genotypes and subtypes are detected with the same assay. Amplification nucleation site analysis may address this, as there is no time dependency. Crude sample preparation with remnant inhibitors/confounders can also adversely affect traditional amplification quantification, though it is not yet clear if this will impact the quantification accuracy of amplification nucleation site counting. The impact of primer mismatches and sample preparation is the focus on future work.

Mobile phone- and inexpensive-based fluorescence readers have been used to detect and quantify isothermal amplification assays, typically using either endpoint fluorescence or time-to-threshold values.[46,57,59,60] Mobile phone or inexpensive optical component based readers may be appealing for a POC setting because they potentially result in lower costs and greater accessibility. However, it is well known that differences in phone components (*i.e.* camera quality and/or flash spectrum) can result in differing signals,[61,62] potentially confounding quantification if not properly calibrated. Amplification nucleation site analysis does not rely on relative fluorescence or precise pixel intensity values and may prove to be a more robust and consistent method of quantification across inexpensive optics as well as mobile phone types and models.

4. Summary

We present a novel method for HIV-1 DNA and RNA nucleic acid quantification using paper-based isothermal amplification and nucleation site amplification counting. We observe discrete fluorescent amplification nucleation sites when recombinase polymerase amplification is performed on porous fiber substrates and use an image analysis algorithm

Table 2 Performance of amplification nucleation site analysis *vs.* tube-based RPA

	Log (input copies per reaction)	Average predicted concentration (log)	
		Tube-based time-to-threshold analysis	Amplification nucleation site analysis
HIV-1 DNA	3.48	3.18 (±0.05)	3.39 (±0.16)
	3	3.13 (±0.14)	3.09 (±0.10)
	2.48	2.76 (±0.01)	2.55 (±0.19)
	2	2.22 (±0.58)	1.93 (±0.13)
	Average absolute error	0.33 (±0.19)	0.14 (±0.09)
HIV-1 RNA	3.48	3.36 (±0.03)	3.35 (±0.20)
	3	2.89 (±0.03)	3.03 (±0.07)
	2.7	2.83 (±0.08)	2.72 (±0.07)
	2	2.65 (±0.30)	1.95 (±0.32)
	Average absolute error	0.25 (±0.28)	0.16 (±0.13)

to count the sites. The number of amplification sites follows a power law relation to the number of input nucleic acid copies. Using DNA targets, we report a quantifiable range of 67–3000 cps rxn^{-1}, as higher copy concentrations lead to significant amplification nucleation site merging and difficulty in site quantification using our algorithms. With HIV-1 RNA targets, we show well-defined correlation between nucleation sites and input copies between 50–3000 cps rxn^{-1}. The amplification process takes less than 20 minutes at a single temperature with inexpensive materials and minimal user steps, and we believe that amplification nucleation site analysis could be leveraged in low-cost point-of-care nucleic acid amplification tests to provide more robust isothermal nucleic acid amplification quantification ability compared to current methods. We also present a mobile phone-based imaging system that is able to quantify amplification nucleation sites with a custom onboard processing app with similar performance to that of a microscope-based setup, suggesting that mobile phone-based amplification nucleation site analysis is a viable strategy for point-of-care applications. Future work includes extending the quantifiable range, further comparing the precision and accuracy of this method to tube-based RPA, and verifying the system using clinical samples across genotypes.

We observe merging of nucleation sites at higher concentrations of target that limits the quantifiable range of our approach. There are several ways to improve the dynamic range. Improved image analysis algorithms, perhaps one using pattern recognition over time, may extend the quantifiable range by resolving additional nucleation sites that are currently difficult to discern from site merging effects. The effective dynamic range of the system can be shifted by dilution of the sample, allowing for higher concentrations of target to be quantified. Using this dilution approach, multiple amplification pads could be used to extend the dynamic range, particularly if the expected copy number order of magnitude is not known *a priori*. This dilution scheme with multiple parallel experiments is frequently used in ddPCR. Our preliminary experiments show that increasing the area of the amplification pad (*e.g.* through tripling the reaction volume while keeping the nucleic acid copy number per reaction constant) can increase the dynamic range, as it effectively reduces the amplification nucleation site density.

There is an inherent tradeoff in analytical techniques between reducing cost and complexity and decrease in performance. Amplification nucleation site analysis has a more limited dynamic range than qPCR or digital isothermal methods; however, the simplicity and potential for lower cost compared to other techniques may ultimately meet target product profiles. This is particularly true in an application spaces where pathogen concentrations are relatively low, such as in HIV viral load monitoring, where sample quantification is particularly valued near traditional cutoffs of 1000 copies of HIV RNA per mL of plasma for antiretroviral efficacy determination.[10] Further optimization of membrane properties may also be useful in improving the limit-of-detection, as the important characteristics and properties of different membrane types in relation to their ability to sustain amplification reactions is still unclear.

We hypothesize that the RPA grouping agents, which increase the reaction fluid's bulk viscosity, are crucial in the formation of individual nucleation sites. For this reason, we do not expect this method will be possible with other native isothermal amplification chemistries; however, it may be possible to increase the viscosity of other amplification techniques (*e.g.* LAMP) through grouping agents with similar results.

The amplification nucleation site analysis method presented here can be integrated with most nucleic acid amplification sample preparation workflows to be used at the point-of-care. Each disease target has specific sample preparation requirements. For example, viral detection in blood samples, such as HIV, requires viral envelope lysis, cell fractionation, RNase deactivation, and purification from amplification inhibitors (such as heme).[10] In nearly all commercial molecular assays the cell filtration is performed by centrifugation and RNase deactivation nucleic acid extraction is accomplished by solid phase extraction in high molarity chaotropic salts. We have developed novel chemistry and paper-based cell filtration and nucleic acid extraction techniques that are compatible with the point-of-care and avoid the use of chaotropic salts.[63,64] Viral detection in nasal and saliva samples, such as SARS-CoV-2 testing, can be accomplished at the POC with minimal sample preparation by direct addition of the sample into viral transport media with a lysis surfactant and reducing agent (such as DTT).[51,65,66] Integration of sample preparation with the presented quantitative nucleic acid amplification is the focus of our future work.

Author contributions

Benjamin P. Sullivan: conceptualization, methodology, investigation, writing – original draft, writing – review & editing. Yu-Shan Chou: methodology, investigation. Andrew T. Bender: conceptualization, methodology, writing – review & editing. Coleman D. Martin: conceptualization, methodology, investigation. Zoe G. Kaputa: methodology, investigation. Hugh March: methodology, investigation. Minyung Song: methodology, investigation. Jonathan D. Posner: conceptualization, writing – review & editing, supervision, project administration, funding acquisition.

Conflicts of interest

There are no conflicts of interest to declare.

Acknowledgements

We would like to gratefully acknowledge Dr. Lorraine Lillis and Dr. David Boyle (PATH) for their work in providing the viral RNA used in this manuscript. We would also like to

acknowledge Luke Orr from the Cole DeForest Lab and Ross Nelson from the Jonathan Posner Lab at the University of Washington for initial discussions regarding the smartphone nucleation site counting algorithm. The work reported in this publication was supported by the National Institute of Biomedical Imaging and Bioengineering of the National Institutes of Health under Award Number R01EB022630 and by the National Center for Advancing Translational Sciences of the National Institutes of Health under Award Number TL1TR002318. Part of this work was conducting using equipment in the Biochemical Diagnostics Foundry for Translational Research supported by the M. J. Murdock Charitable Trust. The content is solely the responsibility of the authors and does not necessarily represent the official views of the National Institutes of Health.

References

1 S. Attia, M. Egger, M. Müller, M. Zwahlen and N. Low, Sexual transmission of HIV according to viral load and antiretroviral therapy: systematic review and meta-analysis, *AIDS*, 2009, **23**(11), 1397–1404.

2 J. LeMessurier, G. Traversy, O. Varsaneux, M. Weekes, M. T. Avey and O. Niragira, *et al.*, Risk of sexual transmission of human immunodeficiency virus with antiretroviral therapy, suppressed viral load and condom use: a systematic review, *CMAJ*, 2018, **190**(46), E1350–E1360.

3 Antiretroviral Therapy Cohort Collaboration, Survival of HIV-positive patients starting antiretroviral therapy between 1996 and 2013: a collaborative analysis of cohort studies, *Lancet*, 2017, **4**(8), e349–e356.

4 A. Singanayagam, M. Patel, A. Charlett, J. Lopez Bernal, V. Saliba and J. Ellis, *et al.*, Duration of infectiousness and correlation with RT-PCR cycle threshold values in cases of COVID-19, England, January to May 2020, *Eurosurveillance*, 2020, **25**(32), 2001483, Available from: **https://www.ncbi.nlm.nih.gov/pmc/articles/PMC7427302/**.

5 R. Jaafar, S. Aherfi, N. Wurtz, C. Grimaldier, T. Van Hoang, P. Colson, D. Raoult and B. La Scola, Correlation Between 3790 Quantitative Polymerase Chain Reaction–Positives Samples and Positive Cell Cultures, Including 1941 Severe Acute Respiratory Syndrome Coronavirus 2 Isolates, *Clin. Infect. Dis.*, 2021, **72**(11), e921.

6 B. Vogelstein and K. W. Kinzler, Digital PCR, *Proc. Natl. Acad. Sci. U. S. A.*, 1999, **96**(16), 9236–9241.

7 B. J. Hindson, K. D. Ness, D. A. Masquelier, P. Belgrader, N. J. Heredia and A. J. Makarewicz, *et al.*, High-Throughput Droplet Digital PCR System for Absolute Quantitation of DNA Copy Number, *Anal. Chem.*, 2011, **83**(22), 8604–8610.

8 QX200 Droplet Digital PCR System, [cited 2021 Nov 18], Available from: **https://www.bio-rad.com/sites/default/files/webroot/web/pdf/lsr/literature/Bulletin_6311.pdf**.

9 A. Niemz, T. M. Ferguson and D. S. Boyle, Point-of-care nucleic acid testing for infectious diseases, *Trends Biotechnol.*, 2011, **29**(5), 240–250.

10 P. Drain, J. Dorward, A. Bender, L. Lillis and F. Marinucci, Point-of-care HIV viral load testing: An essential tool for a sustainable global HIV/AIDS response, *Clin. Microbiol. Rev.*, 2018, **32**(3), e00097-18.

11 P. K. Drain, E. P. Hyle, F. Noubary, K. A. Freedberg, D. Wilson and W. R. Bishai, *et al.*, Diagnostic point-of-care tests in resource-limited settings, *Lancet Infect. Dis.*, 2014, **14**(3), 239–249.

12 R. W. Peeling and D. Mabey, Point-of-care tests for diagnosing infections in the developing world, *Clin. Microbiol. Infect.*, 2010, **16**(8), 1062–1069.

13 J. Li, J. Macdonald and F. von Stetten, Review: a comprehensive summary of a decade development of the recombinase polymerase amplification, *Analyst*, 2018, **144**(1), 31–67.

14 Y. Mori, M. Kitao, N. Tomita and T. Notomi, Real-time turbidimetry of LAMP reaction for quantifying template DNA, *J. Biochem. Biophys. Methods*, 2004, **59**(2), 145–157.

15 S. Roy, N. F. Mohd-Naim, M. Safavieh and M. U. Ahmed, Colorimetric Nucleic Acid Detection on Paper Microchip Using Loop Mediated Isothermal Amplification and Crystal Violet Dye, *ACS Sens.*, 2017, **2**(11), 1713–1720.

16 A. A. E. Wahed, P. Patel, O. Faye, S. Thaloengsok, D. Heidenreich and P. Matangkasombut, *et al.*, Recombinase Polymerase Amplification Assay for Rapid Diagnostics of Dengue Infection, *PLoS One*, 2015, **10**(6), e0129682.

17 M. Euler, Y. Wang, O. Nentwich, O. Piepenburg, F. T. Hufert and M. Weidmann, Recombinase polymerase amplification assay for rapid detection of Rift Valley fever virus, *J. Clin. Virol.*, 2012, **54**(4), 308–312.

18 A. Abd El Wahed, P. Patel, D. Heidenreich, F. T. Hufert and M. Weidmann, Reverse Transcription Recombinase Polymerase Amplification Assay for the Detection of Middle East Respiratory Syndrome Coronavirus, *PLoS Curr*, 2013, **5**, 5, Available from: **https://www.ncbi.nlm.nih.gov/pmc/articles/PMC3871419/**.

19 L. Lillis, D. A. Lehman, J. B. Siverson, J. Weis, J. Cantera and M. Parker, *et al.*, Cross-subtype detection of HIV-1 using reverse transcription and recombinase polymerase amplification, *J. Virol. Methods*, 2016, **230**, 28–35.

20 Z. A. Crannell, B. Rohrman and R. Richards-Kortum, Quantification of HIV-1 DNA Using Real-Time Recombinase Polymerase Amplification, *Anal. Chem.*, 2014, **86**(12), 5615–5619.

21 A. T. Bender, M. D. Borysiak, A. M. Levenson, L. Lillis, D. S. Boyle and J. D. Posner, Semiquantitative Nucleic Acid Test with Simultaneous Isotachophoretic Extraction and Amplification, *Anal. Chem.*, 2018, **90**(12), 7221–7229.

22 F. Shen, E. K. Davydova, W. Du, J. E. Kreutz, O. Piepenburg and R. F. Ismagilov, Digital Isothermal Quantification of Nucleic Acids via Simultaneous Chemical Initiation of Recombinase Polymerase Amplification Reactions on SlipChip, *Anal. Chem.*, 2011, **83**(9), 3533–3540.

23 Z. Li, Y. Liu, Q. Wei, Y. Liu, W. Liu and X. Zhang, *et al.*, Picoliter Well Array Chip-Based Digital Recombinase Polymerase Amplification for Absolute Quantification of Nucleic Acids, *PLoS One*, 2016, **11**(4), e0153359.

24 X. Lin, X. Huang, K. Urmann, X. Xie and M. R. Hoffmann, Digital Loop-Mediated Isothermal Amplification on a Commercial Membrane, *ACS Sens.*, 2019, **4**(1), 242–249.
25 L. Mazutis, A. F. Araghi, O. J. Miller, J.-C. Baret, L. Frenz and A. Janoshazi, *et al.*, Droplet-Based Microfluidic Systems for High-Throughput Single DNA Molecule Isothermal Amplification and Analysis, *Anal. Chem.*, 2009, **81**(12), 4813–4821.
26 A. Gansen, A. M. Herrick, I. K. Dimov, L. P. Lee and D. T. Chiu, Digital LAMP in a sample self-digitization (SD) chip, *Lab Chip*, 2012, **12**(12), 2247–2254.
27 H. Ahn, B. S. Batule, Y. Seok and M.-G. Kim, Single-Step Recombinase Polymerase Amplification Assay Based on a Paper Chip for Simultaneous Detection of Multiple Foodborne Pathogens, *Anal. Chem.*, 2018, **90**(17), 10211–10216.
28 B. A. Rohrman and R. R. Richards-Kortum, A paper and plastic device for performing recombinase polymerase amplification of HIV DNA, *Lab Chip*, 2012, **12**(17), 3082–3088.
29 Y. Seok, H.-A. Joung, J.-Y. Byun, H.-S. Jeon, S. J. Shin and S. Kim, *et al.*, A Paper-Based Device for Performing Loop-Mediated Isothermal Amplification with Real-Time Simultaneous Detection of Multiple DNA Targets, *Theranostics*, 2017, **7**(8), 2220–2230.
30 L. K. Lafleur, J. D. Bishop, E. K. Heiniger, R. P. Gallagher, M. D. Wheeler and P. Kauffman, *et al.*, A rapid, instrument-free, sample-to-result nucleic acid amplification test, *Lab Chip*, 2016, **16**(19), 3777–3787.
31 L. Magro, B. Jacquelin, C. Escadafal, P. Garneret, A. Kwasiborski and J.-C. Manuguerra, *et al.*, Paper-based RNA detection and multiplexed analysis for Ebola virus diagnostics, *Sci. Rep.*, 2017, **7**, 1347.
32 E. A. Phillips, T. J. Moehling, K. F. K. Ejendal, O. S. Hoilett, K. M. Byers and L. A. Basing, *et al.*, Microfluidic rapid and autonomous analytical device (microRAAD) to detect HIV from whole blood samples, *Lab Chip*, 2019, **19**, 3375–3386, Available from: **http://pubs.rsc.org/en/content/articlelanding/2019/lc/c9lc00506d**.
33 I. T. Hull, E. C. Kline, G. K. Gulati, J. H. Kotnik, N. Panpradist and K. G. Shah, *et al.*, Isothermal Amplification with a Target-Mimicking Internal Control and Quantitative Lateral Flow Readout for Rapid HIV Viral Load Testing in Low-Resource Settings, *Anal. Chem.*, 2022, **94**(2), 1011–1021.
34 C. P. Mancuso, Z.-X. Lu, J. Qian, S. A. Boswell and M. Springer, A Semi-Quantitative Isothermal Diagnostic Assay Utilizing Competitive Amplification, *Anal. Chem.*, 2021, **93**(27), 9541–9548.
35 B. A. Rohrman, V. Leautaud, E. Molyneux and R. R. Richards-Kortum, A Lateral Flow Assay for Quantitative Detection of Amplified HIV-1 RNA, *PLoS One*, 2012, **7**(9), e45611.
36 D. Lee, Y. Shin, S. Chung, K. S. Hwang, D. S. Yoon and J. H. Lee, Simple and Highly Sensitive Molecular Diagnosis of Zika Virus by Lateral Flow Assays, *Anal. Chem.*, 2016, **88**(24), 12272–12278.
37 J. R. Choi, J. Hu, R. Tang, Y. Gong, S. Feng and H. Ren, *et al.*, An integrated paper-based sample-to-answer biosensor for nucleic acid testing at the point of care, *Lab Chip*, 2016, **16**(3), 611–621.
38 J. M. Rosenbohm, C. M. Klapperich and M. Cabodi, Tunable Duplex Semiquantitative Detection of Nucleic Acids with a Visual Lateral Flow Immunoassay Readout, *Anal. Chem.*, 2022, **94**(9), 3956–3962.
39 N. M. Rodriguez, J. C. Linnes, A. Fan, C. K. Ellenson, N. R. Pollock and C. M. Klapperich, Paper-Based RNA Extraction, *in Situ* Isothermal Amplification, and Lateral Flow Detection for Low-Cost, Rapid Diagnosis of Influenza A (H1N1) from Clinical Specimens, *Anal. Chem.*, 2015, **87**(15), 7872–7879.
40 Y. Seok, B. S. Batule and M.-G. Kim, Lab-on-paper for all-in-one molecular diagnostics (LAMDA) of zika, dengue, and chikungunya virus from human serum, *Biosens. Bioelectron.*, 2020, **165**, 112400.
41 M. Liu, Y. Zhao, H. Monshat, Z. Tang, Z. Wu and Q. Zhang, *et al.*, An IoT-enabled paper sensor platform for real-time analysis of isothermal nucleic acid amplification tests, *Biosens. Bioelectron.*, 2020, **169**, 112651.
42 C. Liu, E. Geva, M. Mauk, X. Qiu, W. R. Abrams and D. Malamud, *et al.*, An isothermal amplification reactor with an integrated isolation membrane for point-of-care detection of infectious diseases, *Analyst*, 2011, **136**(10), 2069.
43 A. M. Sanchez, C. T. DeMarco, B. Hora, S. Keinonen, Y. Chen and C. Brinkley, *et al.*, Development of a contemporary globally diverse HIV viral panel by the EQAPOL program, *J. Immunol. Methods*, 2014, **409**, 117–130.
44 J. Schindelin, I. Arganda-Carreras, E. Frise, V. Kaynig, M. Longair and T. Pietzsch, *et al.*, Fiji: an open-source platform for biological-image analysis, *Nat. Methods*, 2012, **9**(7), 676–682.
45 G. Bradski, The OpenCV Library, *Dr Dobb's Journal of Software Tools*, 2000.
46 N. Kaur, J. S. Michael and B. J. Toley, A modular paper-and-plastic device for tuberculosis nucleic acid amplification testing in limited-resource settings, *Sci. Rep.*, 2019, **9**(1), 15367.
47 G. Xu, D. Nolder, J. Reboud, M. C. Oguike, D. A. van Schalkwyk and C. J. Sutherland, *et al.*, Paper-Origami-Based Multiplexed Malaria Diagnostics from Whole Blood, *Angew. Chem.*, 2016, **128**(49), 15476–15479.
48 J. T. Connelly, J. P. Rolland and G. M. Whitesides, "Paper Machine" for Molecular Diagnostics, *Anal. Chem.*, 2015, **87**(15), 7595–7601.
49 L. Lillis, J. Siverson, A. Lee, J. Cantera, M. Parker and O. Piepenburg, *et al.*, Factors influencing Recombinase polymerase amplification (RPA) assay outcomes at point of care, *Mol. Cell. Probes*, 2016, **30**(2), 74–78.
50 O. Piepenburg, C. H. Williams, D. L. Stemple and N. A. Armes, DNA Detection Using Recombination Proteins, *PLoS Biol.*, 2006, **4**(7), e204.

51 Y. Zhu, X. Wu, A. Gu, L. Dobelle, C. A. Cid and J. Li, *et al.*, Membrane-Based In-Gel Loop-Mediated Isothermal Amplification (mgLAMP) System for SARS-CoV-2 Quantification in Environmental Waters, *Environ. Sci. Technol.*, 2022, **56**(2), 862–873.

52 R. D. Mitra and G. M. Church, In situ localized amplification and contact replication of many individual DNA molecules, *Nucleic Acids Res.*, 1999, **27**(24), e34–e39.

53 B. Lutz, T. Liang, E. Fu, S. Ramachandran, P. Kauffman and P. Yager, Dissolvable fluidic time delays for programming multi-step assays in instrument-free paper diagnostics, *Lab Chip*, 2013, **13**(14), 2840–2847.

54 S. R. Krishnan, J. Bal and S. A. Putnam, A simple analytic model for predicting the wicking velocity in micropillar arrays, *Sci. Rep.*, 2019, **9**(1), 20074.

55 J. C. Linnes, N. M. Rodriguez, L. Liu and C. M. Klapperich, Polyethersulfone improves isothermal nucleic acid amplification compared to current paper-based diagnostics, *Biomed. Microdevices*, 2016, **18**(2), 30.

56 E. M. Burd, Validation of Laboratory-Developed Molecular Assays for Infectious Diseases, *Clin. Microbiol. Rev.*, 2010, **23**(3), 550–576.

57 M. D. Borysiak, K. W. Kimura and J. D. Posner, NAIL: Nucleic Acid detection using Isotachophoresis and Loop-mediated isothermal amplification, *Lab Chip*, 2015, **15**(7), 1697–1707.

58 D. S. Boyle, D. A. Lehman, L. Lillis, D. Peterson, M. Singhal and N. Armes, *et al.*, Rapid Detection of HIV-1 Proviral DNA for Early Infant Diagnosis Using Recombinase Polymerase Amplification, *MBio*, 2013, **4**(2), e00135–e001313.

59 J. Song, M. G. Mauk, B. A. Hackett, S. Cherry, H. H. Bau and C. Liu, Instrument-Free Point-of-Care Molecular Detection of Zika Virus, *Anal. Chem.*, 2016, **88**(14), 7289–7294.

60 G. L. Damhorst, C. Duarte-Guevara, W. Chen, T. Ghonge, B. T. Cunningham and R. Bashir, Smartphone-Imaged HIV-1 Reverse-Transcription Loop-Mediated Isothermal Amplification (RT-LAMP) on a Chip from Whole Blood, *Engineering*, 2015, **1**(3), 324–335.

61 K. G. Shah, S. Kumar, V. Singh, L. Hansen, E. Heiniger and J. D. Bishop, *et al.*, Two-Fluorophore Mobile Phone Imaging of Biplexed Real-Time NAATs Overcomes Optical Artifacts in Highly Scattering Porous Media, *Anal. Chem.*, 2020, **92**(19), 13066–13072.

62 D. Lee, W. P. Chou, S. H. Yeh, P. J. Chen and P. H. Chen, DNA detection using commercial mobile phones, *Biosens. Bioelectron.*, 2011, **26**(11), 4349–4354.

63 B. P. Sullivan, A. T. Bender, D. N. Ngyuen, J. Y. Zhang and J. D. Posner, Nucleic acid sample preparation from whole blood in a paper microfluidic device using isotachophoresis, *J. Chromatogr., B*, 2021, **1163**, 122494.

64 A. T. Bender, B. P. Sullivan, L. Lillis and J. D. Posner, Enzymatic and Chemical-Based Methods to Inactivate Endogenous Blood Ribonucleases for Nucleic Acid Diagnostics, *J. Mol. Diagn.*, 2020, **22**(8), 1030–1040.

65 B. Ning, T. Yu, S. Zhang, Z. Huang, D. Tian, Z. Lin, A. Niu, N. Golden, K. Hensley, B. Threeton, C. J. Lyon, X.-M. Yin, C. J. Roy, N. S. Saba, J. Rappaport, Q. Wei and T. Y. Hu, A smartphone-read ultrasensitive and quantitative saliva test for COVID-19, *Sci. Adv.*, 2021, **7**, eabe3703.

66 D. Xiong, W. Dai, J. Gong, G. Li, N. Liu and W. Wu, *et al.*, Rapid detection of SARS-CoV-2 with CRISPR-Cas12a, *PLoS Biol.*, 2020, **18**(12), e3000978.